Spin Pumping and Magnetic Anisotropy in La 2/3 Sr 1/3 MnO 3 /Pt Systems

Ibtissem Benguettat-El Mokhtari, Yves Roussigné, Traian Petrisor, Fatih Zighem, Fatiha Kail, Larbi Chahed, Victor Pierron, Laurence Méchin, Mihai Gabor, Mohamed Belmeguenai

Spin pumping and magnetic anisotropy in $La_{2/3}Sr_{1/3}MnO_3$/Pt systems

Ibtissem Benguettat- EL Mokhtari[1, 2], *Yves Roussigné*[1], *Traian Petrisor jr*[3], *Fatih Zighem*[1], *Fatiha Kail*[2], *Larbi Chahed*[2], *Victor Pierron*[4], *Laurence Méchin*[4], *MihaiGabor*[3] and *Mohamed Belmeguenai* [1,*]

[1]*Université Sorbonne Paris Nord, LSPM, CNRS, UPR 3407, F-93430 Villetaneuse, France*
[2]*Laboratoire de Physique des Couches Minces et Matériaux pour l'Electronique, Université Oran1, BP1524, El M'naouar 31100 Oran, Algérie*
[3]*Center for Superconductivity, Spintronics and Surface Science, Technical University of Cluj-Napoca, Str. Memorandumului No. 28 RO-400114 Cluj-Napoca, ROMANIA*
[4] *Normandie University, UNICAEN, ENSICAEN, CNRS, GREYC, 14000 Caen, France*

Abstract- $La_{2/3}Sr_{1/3}MnO_3$ (LSMO) thin films of various thicknesses (6, 8, 10, 20 and 30 nm), capped by 7 nm thick Pt layer were grown by pulsed laser deposition on $SrTiO_3$ (001) substrates. X-ray diffraction revealed that LSMO films are (001) oriented. Vibrating sample magnetometer was used to determine the magnetization at saturation and the magnetic dead layer thickness. This latter is around 3.4 nm, significantly thicker compared with the one induced at interfaces of Pt with ferromagnetic transition metals. Microstrip line ferromagnetic resonance (MS-FMR) was used to extract the gyromagnetic ratio, which was found to increase with LSMO thickness. MS-FMR revealed that the in-plane magnetic anisotropy is dominated by uniaxial contribution for the Pt capped film while the non-capped 10 nm thick LSMO layer shows fourfold anisotropy. Furthermore, the thickness dependence of effective magnetization revealed that the existence of a second order perpendicular anisotropy term, which is thickness-dependent and of a weak uniaxial interface anisotropy. The Gilbert damping coefficient was found to vary linearly with the inverse of the effective LSMO thickness due to spin pumping leading to relatively low spin mixing conductance of LSMO/Pt interface.

PACS numbers: 75.70.Cn, 75.30.Ds, 75.70.Ak, 75.70.Tj

Keywords: Interface effects, Perpendicular magnetic anisotropy, Brillouin light scattering, spin waves and magnetization dynamics.
* belmeguenai.mohamed@univ-paris13.fr,

I- Introduction

The emergence of spintronics, where both electron spin and charge are used as information vectors, has triggered the research of new materials where the spin polarization rendered by the spin asymmetry at the Fermi level is one of the most important of their properties. Therefore, spintronic application revives the interest in the perovskite manganites, generally referred to as colossal magnetoresistance materials. $La_{2/3}Sr_{1/3}MnO_3$ (LSMO) is an attracting perovskite manganite material because of its low saturation magnetization, its expected spin polarization close to 100% [1] and its low magnetic damping [2], ingredients for low critical current densities in spin transfer torque switching [3]. Damping parameter, governing the magnetization relaxation, is an important technological parameter since it also controls how fast the magnetization reverses. Indeed, depending on the desired application, the damping value should be fixed: low damping is essential for low current densities in spin torque magnetization switching [3] whereas, higher damping values are needed for conventional magnetic recording media such as CoCrPt [4].

Spin pumping [5, 6] is an efficient method to generate a spin current and therefore to tune the magnetic damping in ferromagnetic (FM)/normal metal (NM) based-systems via the choice of FM and NM material and their thicknesses. Spin pumping can be considered as the reciprocal effect of the spin current action on the magnetization: spin current can induce magnetization precession due to the spin transfer torque [7, 8]. Indeed, the magnetization precession (induced by ferromagnetic resonance for example) generates a spin current at the FM/NM interface by transferring the transverse component of spin angular momentum from the FM layer to NM. This spin current diffuses into the NM layer in the direction normal to the interface and is accompanied by spin angular momentum loss in the FM layer which is an additional damping source of magnetization dynamics. The spin pumping phenomenon is governed by the spin mixing conductance parameter

determining the efficiency of this effect at the interface between materials: it determines how much spin current is passed through the interface. Spin pumping in LSMO/Pt system were addressed by Luo et al. [9] and Lee et al. [10]. However, although the LSMO thicknesses were varied by Luo et al., they used conventional ferromagnetic resonance in cavity (X-band), which is limited for the investigation of damping since measurements are made at fixed frequency. In contrast, Lee et al. used a broadband ferromagnetic resonance but the LSMO thickness was fixed to 30 nm and here again the accuracy on spin mixing conductance is questionable. For the precise characterization of spin pumping, broadband technique and variable thicknesses of ferromagnetic layer should be used. Therefore, in this paper, we address the thickness dependence of damping and perpendicular magnetic anisotropy in LSMO/Pt systems. For this, broadband ferromagnetic resonance with microstrip line (MS-FMR) [11], vibrating sample magnetometer (VSM) and x-ray diffraction techniques have been used. We show the presence of a thick magnetic dead layer and that the damping coefficient varies with the inverse of the effective thickness of LSMO films. Moreover, we demonstrated that in contrast to 3d materials in contact with Pt, the perpendicular magnetic anisotropy in LSMO/Pt remains negligible.

II- Samples and experimental techniques

All LSMO films of variable thicknesses (t_{LSMO}= 6, 8, 10 ,20 and 30 nm) were grown on $SrTiO_3$ (STO) (001) substrates using an advanced Pulsed Laser Deposition (PLD) system with in situ RHEED from TSST company with a laser fluence of 1.70 J/cm². The deposition temperature was kept at 750 °C in a pressure of 0.2 mbar of oxygen with a shot frequency of 1 Hz. After deposition, LSMO films were cooled down to room temperature in a 500 mbar O_2 pressure. Next, the samples were transferred to a DC magnetron sputtering chamber without breaking the vacuum for the deposition of the 7 nm thick Pt layer at room temperature in Ar pressure of 4×10^{-2} mbar and at a power of 17.6W. Platinum is used here as the normal metal for spin pumping measurements. It is a heavy metal, which is an efficient spin-sink with a short spin diffusion length. A 10 nm thick uncapped LSMO layer grown in the same conditions is used as a reference sample. X-ray

diffraction (XRD) combined with vibrating sample magnetometer (VSM) have been used to study the structural and the static magnetic properties of the films. Home-made microstrip ferromagnetic resonance (MS-FMR) was used to probe the magnetization dynamics through the investigation of the magnetic damping, gyromagnetic factor and the magnetic anisotropy [11]. In MS-FMR experiment, the magnetic sample is mounted on a microstrip line which is connected to a Hewlett-Packard microwave generator (83752B), operating in the range 0.01-20 GHz and to a Schottky detector used to measure the transmitted power. For each driven microwave frequency, the sample is swept through the resonance by varying the applied external field (up 2.3 kOe for in-plane or up to 15 kOe for out-of-plane applied magnetic fields). In addition, the external magnetic field is modulated at 170 Hz by small (4 Oe) alternating magnetic field allowing lock-in detection via a lock-in amplifier (Stanford research system SR830). The in-plane and the out-of-plane angular dependences measurements are ensured by rotating the sample via motors: in the plane, the sample is mounted on a rod connected to a motor, which ensures vertical translation before and after each rotation to bring the sample far from and into contact with the fixed microstrip line, respectively. For out-of-plane measurements, the sample is directly fixed on the microstrip line and the whole set is connected to a motor which ensures the rotation in the gap of the electromagnet. All the measurements presented below were carried out at room temperature.

III- Results and discussion

1- x-ray diffraction

Figure 1 shows the 2θ/ω x-ray diffraction patterns measured for 30 nm thick LSMO sample capped with Pt. The patterns indicate the presence of the (00l) type LSMO and STO substrate peaks. This confirms the expected epitaxial growth of the LSMO layer on the single crystal STO (001) substrate, which is (001)LSMO||(001)STO and [001]LSMO||[001]STO. The LSMO out-of-plane lattice parameter was evaluated to be 3.84 Å. The calculated lattice parameter, which is less than the pseudo-cubic LSMO unit cell parameter, a_{LSMO} =3.867 Å [12], suggests the presence of an in-plane tensile strain in the LSMO thin film. This is because the STO lattice parameter is a_{STO} =

3.905 Å and an in-plane matched growth of the film results in the in-plane elongation of the film lattice, which in turn produces an out-of-plane compression. Moreover, the x-ray pattern presents a Pt (111) peak, originating from the Pt capping layer. To better visualize this peak, we have also performed a $2\theta/\omega$ diffractogram, with an out-of-plane 0.4° angle offset (not shown here). This resulted in the reduction of the additional substrate artefact peaks induced by the fact that the X-rays used here are not monochromatic. The growth of LSMO capped with Pt is thus similar to that of the uncapped LSMO [13] and is in agreement with previous investigations [9, 10].

2-Static magnetic properties

For the precise determination of perpendicular magnetic anisotropy (PMA) and spin mixing conductance, the magnetization at saturation (M_s) and the eventual magnetic dead layer thickness (t_d) should be first evaluated. These two quantities are straightforwardly determined by VSM technique from the thickness dependence of the areal magnetic moment. Figure 2 shows the LSMO thickness (t_{LSMO}) dependences of the saturation magnetic moment per unit area ($M_s \times t_{LSMO}$) for LSMO/ Pt system. M_s and t_d are determined from the linear fits of these data: the slope gives M_s and t_d corresponds to the horizontal axis intercept. The magnetic dead layer of 3.4±0.2 nm remains within the range given by Angeloni et al. [14] and Huijben et al. [15] for LSMO/STO systems but it is thicker than the reported values in references [9] (1.7 nm) and [16] (1.4 nm). Although a thickness dependence of the areal magnetic moment is used in [9], t_d was determined from the temperature dependence of 7.2 nm thick LSMO layer. The magnetization at saturation M_s=323±19 emu/cm^3 is in good agreement to the reported one in [9, 15] and is higher than the given one (265 emu/cm^3) in [10]. This magnetic dead layer refers to the region at the surface or at the interface with the substrate and capping layer where the ferromagnetic properties of the manganite are greatly diminished or modified. The origin of this magnetic dead layer is still unclear and under debate, making it the subject of several researches over the last few years. It has been suggested that the dead layer likely contains oxygen vacancies which disrupt exchange coupling and hence destroy

long range order [17]. In the following, the obtained values of M_s (M_s =323 ±19 emu/cm^3) and t_d (t_d =3.4±0.2 nm) will be used to calculate all the magnetic parameters presented in this study.

3-Dynamic magnetic properties

In this section, we focus on the investigation of PMA and Gilbert damping versus LSMO thicknesses. In the following, we consider the effective thickness of LSMO (t_{eff}=t_{LSMO}-t_d) defined as the nominal LSMO thickness (t_{LSMO}) reduced by the magnetic dead layer thickness. In this study, MS-FMR under in-plane and perpendicular-to-plane applied magnetic fields were used. Typical MS-FMR spectra are shown in figure 3a for the LSMO (8 nm)/Pt under in-plane applied magnetic field, where the recorded signal is proportional to the field derivative of the absorbed power as a function of the applied magnetic field. By fitting these experimental spectra using equation (1) [18], one can obtain the resonance field and the FMR linewidth which will be exploited in this section.

$$\frac{dP_{ab}}{dH} = A_0 \frac{-2\Delta H(H-H_R)\cos(\delta)+[\Delta H^2-(H-H_R)^2]\sin(\delta)}{[\Delta H^2-(H-H_R)^2]^2} + A_1 \quad (1)$$

Where P_{ab} is the absorbed power, δ denotes the mixing angle between dispersive and dissipative components, A_0 is the amplitude, A_1 is an offset value, H_R is the resonance field and ΔH is the half linewidth at half maximum. Note that the fitted experimental data with equation (1) allows deducing ΔH.

Besides M_s and t_d, the g value, which determines the gyromagnetic ratio (γ) is also needed, for the precise determination of the Gilbert damping, the spin mixing conductance and the magnetic anisotropy. For this purpose, we first investigated the frequency variations versus the amplitude of the perpendicular to the film applied magnetic field as shown in figure 3b for various LSMO thicknesses. The observed linear dependence of the frequency versus the perpendicular applied field (θ_H=θ_M=0°) is consistent with equation (2) and allows to deduce the gyromagnetic ratio $\gamma/(2\pi)$ from the slope of the linear fit of the experimental data (figure 3b).

$$f_{Out} = \frac{\gamma}{2\pi}\sqrt{\begin{matrix}\left[Hcos(\theta_M - \theta_H) - 4\pi M_{eff}\cos(2\theta_M) + \frac{2K_{\perp 2}}{M_s}\left(cos(2\theta_M) + cos(4\theta_M)\right)\right] \\ \left[Hcos(\theta_M - \theta_H) - 4\pi M_{eff}cos^2(\theta_M) + \frac{4K_{\perp 2}}{M_s}cos^4(\theta_M)\right]\end{matrix}} \quad (2)$$

Where f_{Out} is the frequency of the uniform precession mode for out-of-plane applied magnetic field, $4\pi M_{eff//} = 4\pi M_{eff} = 4\pi M_s - \frac{2K_\perp}{M_s}$ the effective magnetization out-of-plane, $K_\perp$ is the effective perpendicular uniaxial anisotropy constant and θ_M (θ_H) refers to the out-of-plane angle defining the direction of the magnetization (the applied field) and the normal to the film plane: θ_H=0° corresponds to a magnetic field applied perpendicular to the film plane. We also introduce $4\pi M_{eff\perp} = 4\pi M_s - \frac{2K_\perp}{M_s} - \frac{4K_{\perp 2}}{M_s}$, where $K_{\perp 2}$ is second-order perpendicular magnetic anisotropy constant and its inclusion in equations will be justified below.

The inset in figure 3b shows the thickness dependence of the g-factor (Landé factor), determined from the obtained values of γ/(2π) ($\frac{\gamma}{2\pi}$.=g×13.97 GHz/T). The g-factor decreases with decreasing thickness, consistent with previous studies in metallic thin films [19, 20]. For the larger thickness, the value of the g-factor is 2.11±0.012, which gives an estimation of the bulk value. One should note the slow thickness variation of the g-factor for thick LSMO films (beyond 20 nm) confirming again that the g-factor value of bulk LSMO is around 2.11±0.012. Moreover, the g-factor decreases as the thickness decreases to reach 2.04±0.01, which is close to the free electron value indicating a small spin-orbit interaction [21]. It is worth mentioning that the g-factor is known to depend on composition and is strongly influenced by surface and interface effects, as it depends on the local symmetry [21]. Such interface effects may lead to strong enhancements of the ratio of the orbital to spin angular momentum, which is related to the g-factor. Similar trend was observed in Permalloy [22], which attributed to the orbital motion of electrons not being entirely quenched at surface and interface due to the broken inversion symmetry at interface.

In the following, we employ MS-FMR to investigate both the in-plane and the out-of-plane angular dependences of the resonance field. Figure 4a shows the out-of-plane angular dependence

of the resonance field, at 7 GHz microwave driven frequency, of LSMO thin films of various thicknesses with or without Pt capping layer. During the measurements, the samples were rotated by 180° (with the step of 5°) from in-plane direction (θ_H=±90°) to the normal to the layer plane (θ_H=0°). Maxima and minima of the FMR resonant field clearly identify the hard and easy axes of magnetization. The angular behavior is dominated by a uniaxial perpendicular effective anisotropy with an in-plane easy axis and will be discussed below. Figure 4b shows the typical in-plane angular dependence of the resonance field, at 5 GHz microwave driven frequency, of LSMO(8 nm)/Pt and 10 nm thick uncapped LSMO layer (reference sample). The small variation of the resonance field as a function of the in-plane angle confirms that the anisotropy fields are small and can be neglected at high applied magnetic fields [out-of-plane FMR measurements, justifying the neglected in-plane anisotropy in equation (2)]. This in-plane angular dependence shows that the 10 nm thick uncapped LSMO films exhibits a clear predominant fourfold magnetic anisotropy along the substrate edges ([100] and [010] axes) besides a uniaxial anisotropy along one of the substrate axes. The anisotropy axes are straightforward deduced from minima of the resonance field. It is well known that LSMO films grown on STO(001) present a an in-plane fourfold anisotropy with the easy axes along the [110] and [$1\bar{1}0$] (at 45° with respect to the substrate edges), which was correlated with the full in-plane epitaxy of LSMO and STO [13, 23, 24]. In this case, the fourfold anisotropy has been attributed to a magnetocrystalline origin. Moreover, Vila-Fungueirino et al. [25] reported that LSMO films grown on STO(001) present a fourfold magnetocrystalline anisotropy with an easy axis along [110] superimposed to an order of magnitude smaller uniaxial anisotropy. The monoclinically distorted unit cell of LSMO produces an important difference in the magnitude of the orbital overlap along the equivalent [110] easy axis directions, introducing the extra uniaxial anisotropy term [25]. It is worth to mention that the magnetic anisotropy of the LSMO thin films is very sensitive to the symmetry and morphology of the substrate and that lattice strains can induce an additional anisotropy along the direction of tensile strain [26]. The observed uniaxial anisotropy could also be induced by the substrate morphology, i.e., residual substrate steps

due to miscut angle [27]. The in-plane angular dependence of the STO/LSMO(8 nm)/Pt system seems to be governed by a uniaxial anisotropy. However, a careful observation of this angular dependence allow us to observe that the behavior is not a pure sinusoidal suggesting the existence of other anisotropy terms. Therefore, for the precise determination of the various contributions to the in-plane anisotropy, the angular behavior of the resonance field has been fitted with equation (3).

$$f_{//}^{\ 2} = \left(\frac{\gamma}{2\pi}\right)^2 \left[Hcos(\varphi_M - \varphi_H) + H_u \cos\ 2(\varphi_M - \varphi_u) + \frac{2K_4}{M_S}(\cos 4\ (\varphi_M - \varphi_4)\right] \left[Hcos(\varphi_M - \varphi_H) + 4\pi M_{eff} + \frac{H_u}{2}(1 + cos2(\varphi_M - \varphi_u)) + \frac{K_4}{2M_S}(3 + cos4(\varphi_M - \varphi_4))\right] \quad (3)$$

Where, $f_{//}$ is the frequency of the uniform precession mode for in-plane applied magnetic field, H_u is the uniaxial anisotropy, φ_M is the in–plane direction of the magnetization, φ_u and φ_4 refer respectively to the angle of easy axis direction for the uniaxial and the biaxial anisotropies with the substrate edges. The fourfold in-plane anisotropy field is defined as $H_4 = \frac{4K_4}{M_S}$.

Indeed, the best fits revealed the angular dependence of STO/LSMO(8 nm)/Pt result from the contribution of a fourfold magnetic anisotropy field H_4=7±0.5 Oe [K_4=(0.57±0.07)×10^3 erg/cm^3] with easy axes along [110] and [1$\bar{1}$0] superimposed to a higher a uniaxial field [H_u=16.75±1 Oe, K_u=(2.7±0.29) ×10^3 erg/cm^3] along one edge of the STO substrate. For the STO/LSMO (10 nm) reference sample (uncapped layer), the in-plane angular dependence has been fitted with H_4=16±1 Oe [K_4=(1.29±0.14)×10^3 erg/cm^3] with the easy axes along [100] and equivalent directions and uniaxial anisotropy field of 4±0.3 Oe [K_u=(0.64±0.073) ×10^3 erg/cm^3]. We should mention that no significant fourfold anisotropy has been detected in all the studied LSMO/Pt and the in-plane anisotropy remains weak and below 16 Oe. Similar trends (uniaxial in-plane dominated anisotropy) were reported for LSMO/STO [9, 10].

We will now focus on the perpendicular anisotropy. This can be determined through the investigation of the effective magnetization. Therefore, the uniform precession mode frequencies versus the perpendicular and the in-plane applied magnetic fields (figure 4c for a given φ_H

mentioned in the caption) have been fitted using equations (2) and (3), respectively. The obtained values of the effective magnetization ($M_{eff//}$ and $M_{eff\perp}$ for in-plane and perpendicular to the plane applied magnetic field, respectively) shown in figure 4d versus the reciprocal LSMO effective thickness are significantly different. This difference suggests the existence of a second-order anisotropy term characterized by the constant $K_{\perp 2}$ to be added to the conventional uniaxial perpendicular anisotropy term as indicated in equation (2). According to equation (2) and for in-plane applied magnetic field (θ_H=90°), the contribution of $K_{\perp 2}$ to the frequency vanishes and the fit of experimental data (figure 4c) lead to $4\pi M_{eff//}$. Therefore, measurements under in-plane magnetic field are independent of $K_{\perp 2}$. For perpendicular applied magnetic field (θ_H=0°), the frequency varies linearly versus the applied magnetic field (figure 3b) and the horizontal axis intercept gives $4\pi M_{eff//} - \frac{4K_{\perp 2}}{M_s}$. Therefore, the uniaxial and the second order anisotropy perpendicular constants have been deduced by combining the MS-FMR measurements of the resonance frequency versus in-plane (figure 4c) and perpendicular applied field (figure 3b). The accuracy on these values of $K_{\perp 2}$ has been checked by fitting the out-of-plane angular dependence of the resonance field using equation (2) where a good agreement is observed (figure 4a). We should mention that the out-of-plane angular dependence of resonance field (shown in figure 4a) could not be fitted without the use of $K_{\perp 2}$. The obtained values of $K_{\perp 2}$ (shown in the inset of figure 4d) increase (in absolute value) with the increasing LSMO thickness, suggesting the existence of interface contributions. Note the negative sign of the second order term of the perpendicular anisotropy reinforcing the in-plane easy axis of the magnetization. This second order anisotropy term can arise due to peculiarities of atomic structure at the interface or as a result of non-uniform mechanical stresses existing at interfaces presenting a large crystallographic mismatch [28]. Moreover, B. Dieny et al. have shown analytically that spatial fluctuations of the film thickness can lead to a higher order term if the period of the fluctuations is lower than the exchange length of FM material [28, 29]. Furthermore, both $M_{eff//}$ and $M_{eff//\perp}$ decrease linearly with the reciprocal LSMO thickness, suggesting the existence

of an interface contribution. We will now focus on the uniaxial perpendicular anisotropy constant $K_{\perp}$. This latter obeys the relation $K_{\perp} = K_v + \frac{K_s}{t_{eff}}$ .Therefore, the linear fit of the thickness dependence of $M_{eff//}$ (shown in figure 4d and extracted from the experimental data of figure 4c: measurements under in-plane applied magnetic field) has been used for the determination of the perpendicular uniaxial surface K_s and the volume anisotropy K_v constants from the slope and the intercept with the vertical axis, respectively. The obtained value of K_s=0.03±0.004 erg/cm^2 is negligible and very low, suggesting that the interface contribution to the perpendicular is insignificant, in contrast to the 3d transition metal/Pt systems (such as Pt/Co [27]). The perpendicular volume constant K_v=(-0.57±0.07)×10^5 erg/cm^3 favors the in-plane magnetization and is significantly lower than the reported values [13, 10]. Indeed, by taking into account only $M_{eff//}$, the surface and the volume perpendicular anisotropy constant are underestimated, since the contribution of $K_{\perp 2}$ to both terms is neglected. We thus, used $M_{eff\perp}$ and we deduced the effective surface (K_{seff}=0.055±0.007 erg/cm^2) and volume [K_{veff}=(-2.01±0.035)×10^5 erg/cm^3]. Therefore, while the surface perpendicular anisotropy remains very low compared to that of Co/Pt, the effective volume perpendicular constant is in agreement with the reported values (-2.5×10^5 erg/cm^3 [24] and -4×10^5 erg/cm^3 [10]). The main source of this perpendicular anisotropy is generally considered as proceeding from the interfacial strain through the magnetoelastic coupling [31].

We have also investigated the magnetic damping of the LSMO/Pt samples by measuring the FMR linewidth. Figure 5a shows the typical angular dependence of the half wide at half maximum FMR linewidth (ΔH) of the STO/LSMO(10 nm) and STO/LSMO(8 nm)/Pt samples at 5 GHz microwave driven frequency. The pronounced anisotropy of the linewidth is in disagreement with the intrinsic isotropic Gilbert damping and it must be due to additional extrinsic damping mechanisms. In our samples, extrinsic contributions results mainly from two magnon scattering and mosaicity [32]. In fact, for the STO/LSMO(10 nm), ΔH shows the same fourfold symmetry (four maxima) as it is observed for the angular dependence of the resonance field. In the case of the

STO/LSMO(8 nm)/Pt, the angular dependence of ΔH shows mainly uniaxial symmetry the with minima directions that correspond to the magnetic anisotropy hard axes. Such behaviour of anisotropy linewidth reflecting the resonance field symmetry is a characteristic of two magnon scattering. This two magnon scattering contribution has been confirmed by the out-of-plane angular dependence of the linewidth (not shown here for sake of simplicity since more theoretical considerations would be required to fit ΔH). Indeed, as we move from in-plane to out-of-plane, ΔH increases drastically before decreasing significantly in the vicinity of the normal direction and reaching its minimum at this perpendicular direction. Furthermore, in our MS-FMR set-up the signal to noise ratio is lower for measurements under perpendicular applied magnetic field, especially for the thinner LSMO films (below 10 nm). Although this ratio ensures the determination of resonance field, it does not warrant precise measurements of the linewidth. We thus limited the measurements with perpendicular applied field to the determination of g-factor and we deduced damping from the in-plane measurements of linewidth (along in-plane applied field direction where ΔH is minimal) since they are more sensitive and faster. This two magnon scatting contribution is correlated to the presence of defects preferentially oriented along specific crystallographic directions, thus leading to an asymmetry. Therefore, angular dependence has been fitted by equation (4) [32] (fit parameters are summarized in table I):

$$\Delta H = \Delta H_0 + \frac{2\pi}{\gamma}\alpha f + \Delta H^{2mag} \quad (4)$$

where ΔH^{2mag} is given by [11]:

$$\Delta H^{2mag} = (\Gamma_0 + \Gamma_2 \cos\, 2(\varphi_H - \varphi_2) + \Gamma_4 \cos\, 4(\varphi_H - \varphi_3)) arcsin\left(\frac{f}{\sqrt{f^2+f_0^2}+f_0}\right)$$

here $f_0=\gamma M_{eff}$, f is the driven frequency, ΔH_0 is the inhomogeneous residual linewidth, α is the Gilbert damping constant, Γ_0, Γ_2 (and φ_2) and Γ_4 (and φ_3) are Coefficient (direction) used to characterize the strength of the two magnon contribution. We should mention that the main aim of this paper is to study the LSMO thickness dependence of Gilbert damping and not different

relaxation mechanisms. Therefore, for each sample the angular dependence of ΔH has been used to determine the applied field direction giving the minimum of the linewidth ΔH, for which the frequency dependence of ΔH is then measured for the sake of the minimization of the extrinsic contributions. In these conditions, the deduced damping from the frequency dependence of ΔH, using equation (4) and the measured gyromagnetic ratio for each sample, is much closer to the Gilbert coefficient. The frequency dependences of ΔH for the various samples are shown in figure 5b for the applied field directions mentioned in the figure caption. The analysis of the angular and frequency dependences of the linewidth has been carried out to deduce the Gilbert damping constants shown in figure 5c versus $1/t_{eff}$. It reveals that α increases linearly with $1/t_{eff}$ thus confirming the interfacial nature of spin pumping in LSMO/Pt. Thus we consider that the total damping is given by $\alpha=\alpha_{LSMO}+\Delta\alpha$, where α_{LSMO} is the Gilbert damping constant of the bulk LSMO and $\Delta\alpha$ is the additional damping introduced by the spin pumping effect [33]. The linear fit of the experimental data of figure 5c allows determining α_{LSMO} and $\Delta\alpha$ from the vertical intercept and the slope respectively, since $\Delta\alpha = \frac{g\mu_B}{4\pi M_s t_{eff}} g^{\uparrow\downarrow}$ [34], where μ_B is the Bohr magneton and $g^{\uparrow\downarrow}$ is the spin mixing conductance of LSMO/Pt interface. The intrinsic damping of bulk LSMO [α_{LSMO}= (3.76±0.09) $\times 10^{-3}$] is slightly higher than the reported one by Lee et al. (1.91×10^{-3}) [10] but it is in good agreement with the obtained value for the reference LSMO(10 nm) layer (3.62±0.08) $\times 10^{-3}$. The obtained spin mixing conductance of the LSMO/Pt interface ($g^{\uparrow\downarrow}$ =4.25± 0.3 nm^{-2}), using M_s=323 emu/cm^3 and g=2.08 (the average value of all samples), is significantly lower than those of Py/Pt (30 nm^{-2} [35]) and Co/Pt (45 nm^{-2} [36]). However, it is comparable to those reported for Pt/YIG (6.9 nm^{-2} [37]) and LSMO/Pt (5.5 nm^{-2} [10]). For this latter, we should mention that the obtained value has been deduced from the measurements of single LSMO(30 nm)/Pt sample making it less accurate.

Conclusion

The thickness dependences of the perpendicular magnetic anisotropy and Gilbert damping constant of LSMO/Pt systems have been investigated. The VSM measurements revealed a low magnetization at saturation with a relatively thick magnetic dead layer, probably due to vacancies which disrupt exchange coupling and hence destroy long range order. The FMR investigations showed the existence of second order perpendicular and weak surface anisotropy constants. Moreover, Pt capping layer enhanced significantly the Gilbert damping leading to moderate spin mixing conductance. Finally we conclude that the low magnetization at saturation combined with the low Gilbert damping make LSMO/Pt good candidate for spintronic devices.

Acknowledgements

This work has been supported by the Conseil regional d'Île-de-France (convention 1763) through the DIM NanoK (BIDUL project).

Stack	ΔH_0(Oe)	α($\times 10^{-3}$)	Γ_0(Oe)	Γ_2(Oe)	Γ_4(Oe)	$4\pi M_{eff}$(kOe)	φ_2(°)	φ_3(°)
LSMO(10 nm)	10±0.5	3.62±0.08	15.35±0.75	0	14±0.5	4.2±0.1		45±2
LSMO(8nm)/Pt	5.7±0.3	7.9±0.25	10.35±1	20±1	4.5±0.75	4.5±0.1	0	0±2

Table I: Parameters used for the best fit of the experimental data for the FMR linewidth of figure 5a.

References

[1] M. Bowen, M. Bibes, A. Barthélémy, J. P. Contour, A. Anane, Y. Lemaître, and A. Fert, Appl. Phys. Lett. 82, 233 (2003).

[2] K. Gilmore, Y. U. Idzerda, and M. D. Stiles. J. Appl. Phys., 103, 07D303 (2008).

[3] L. Liu, C.-F. Pai, Y. Li, H. W. Tseng, D. C. Ralph, and R. A. Buhrman, Science 336, 555 (2012).

[4] N. Inaba, Y. Uesaka, A. Nakamura, M. Futamoto, Y. Sugita, and S. Narishige, IEEE Trans. Magn. 33, 2989 (1997).

[5] Y. Tserkovnyak, A. Brataas, and G. E. W. Bauer, Phys. Rev. B 66, 224403 (2002).

[6] Y. Tserkovnyak, A. Brataas, G. E. W. Bauer, and B. I. Halperin, Rev. Mod. Phys. 77, 137 (2006).

[7] J.C. Slonczewski, J. Magn. Magn. Mater. 159, L1 (1996).

[8] L. Berger, Phys. Rev. B 54, 9353 (1996).

[9] G. Y. Luo, J. G. Lin, W-C. Chiang and C-R. Chang, Sci. Rep. 7, 6612 (2017).

[10] H. K. Lee I. Barsukov, A. G. Swartz, B. Kim, L. Yang, H. Y. Hwang, and I. N. Krivorotov, AIP Advances 6, 055212 (2016).

[11] M. Belmeguenai, H. Tuzcuoglu, M. S. Gabor, T. Petrisor, Jr., C. Tiusan, D. Berling, F. Zighem, T. Chauveau, S. M. Chérif, and P. Moch, Phys. Rev. B 87, 184431 (2013).

[12] Michael C. Martin, G. Shirane, Y. Endoh, K. Hirota, Y. Moritomo, and Y. Tokura, Phys. Rev. B 53, 14285 (1996).

[13] M. Belmeguenai, S. Mercone, C. Adamo, T. Chauveau, L. Méchin, P. Monod, P. Moch and D. G. Schlom, J Nanopart. Res. 13, 5669 (2011).

[14] M. Angeloni, G. Balestrino, N. G. Boggio, P. G. Medaglia, P. Orgiani, and A. Tebano, J. Appl. Phys. 96, 6387 (2004).

[15] M. Huijben, L. W. Martin, Y.-H. Chu, M. B. Holcomb, P. Yu, G. Rijnders, D. H. A. Blank, and R. Ramesh, Phys. Rev. B, 78, 094413 (2008).

[16] N. Mottaghi, M. S. Seehra, R. Trappen, S. Kumari, C-Y. Huang, S. Yousefi, G. B.Cabrera, A. H. Romero and M. B. Holcomb, AIPAdvances 8, 056319 (2018).

[17] R. Peng, H. C. Xu, M. Xia, J. F. Zhao, X. Xie, D. F. Xu, B. P. Xie, and D. L. Feng, Appl. Phys. Lett. 104, 081606 (2014).

[18] M. Belmeguenai, K. Aitoukaci, F. Zighem, M. S. Gabor, T. Petrisor, Jr, R. B. Mos, and C. Tiusan, J Appl. Phys. 123, 113905 (2018).

[19] Shaw J. M., Nembach H. T. and Silva T. J., Phys. Rev. B 87, 054416 (2013)

[20] Beaujour J.-M., Ravelosona D., Tudosa I., Fullerton E. E. and Kent A. D., Phys. Rev. B 80, 180415 (2009).

[21] C. Le Graët, D. Spenato, N. Beaulieu, D. Dekadjevi, J-Ph. Jay, S. Pogossian, Bénédicte Warot-Fonrose, J. Ben Youssef, EuroPhys. Lett. 115, 17002 (2016).

[22] J. P. Nibarger, R. Lopusnik, Z. Celinski and T. J. Silva, Appl. Phys. Lett. 83, 93 (2003).

[23] M. Belmeguenai, S. Mercone, C. Adamo, P. Moch, D. G. Schlom, and P. Monod, J. Appl. Phys. 109, 07C120 (2011).

[24] M. Belmeguenai, S. Mercone, C. Adamo, L. Méchin, C. Fur, P. Monod, P. Moch, and D. G. Schlom, Phys. Rev. B 81, 054410 (2010).

[25] J. M. Vila-Fungueirino, C. Ti. Bui, B. Rivas-Murias, E. Winkler, J. Milano, J. Santiso and F. Rivadulla, J. Phys. D: Appl. Phys. 49 315001(2016).

[26] F. Tsui, MC. Smoak, TK. Nath, CB. Eom, Appl. Phys. Lett. 76, 2421 (2000).

[27] P. Perna, C. Rodrigo, E. Jiménez, F. J. Teran, N. Mikuszeit, L. Méchin, J. Camarero and R. Miranda, J. Appl. Phys.110, 13919 (2011).

[28] A. A. Timopheev, R. Sousa, M. Chshiev, T. Nguyen and B. Dieny, Sc. Rep. 6, 26877. (2016).

[29] B. Dieny and A. Vedyayev, Europhys. Lett. 25, 723 (1994).

[30] P. F, Carcia, J. Appl. Phys. 63, 5066 (1988).

[31] M. Golosovsky, P. Monod, P. K. Muduli, and R. C. Budhani, Phys. Rev. B 76, 184413 (2007).

[32] K. Zakeri, J. Lindner, I. Barsukov, R. Meckenstock, M. Farle, U. von Hörsten, H. Wende, W. Keune, J. Rocker, S. S. Kalarickal, K. Lenz, W. Kuch, and K. Baberschke, Phys. Rev. B 76, 104416 (2007).

[33] H. Nakayama, K. Ando, K. Harii, T. Yoshino, R. Takahashi, Y. Kajiwara, K. Uchida, Y. Fujikawa and E. Saitoh, Phys. Rev. B 85, 144408 (2012).

[34] Y. Tserkovnyak, A. Brataas and B. I. Halperin, Rev. Mod. Phys. 77, 1375 (2005).

[35] W. Zhang, V. Vlaminck, J. E. Pearson, R. Divan, S. D. Bader and A. Hoffman, Appl. Phys. Lett. 103, 242414 (2013).

[36] L. Zhu, C. D. Ralph and R. A. Buhrman ,Phys. Rev. Lett. 123, 057203 (2019).

[37] H. Wang, C. Du, P. C. Hammel and F. Yang, Appl. Phys. Lett. 110, 062402 (2017).

Fig. 1 : Belmeguenai et al.

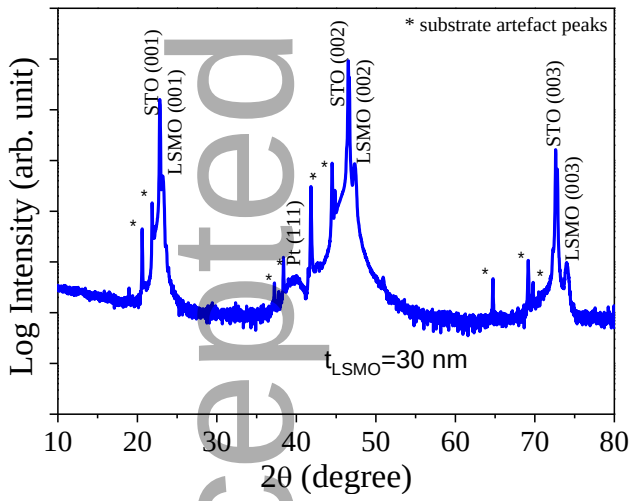

Fig. 2 : Belmeguenai et al.

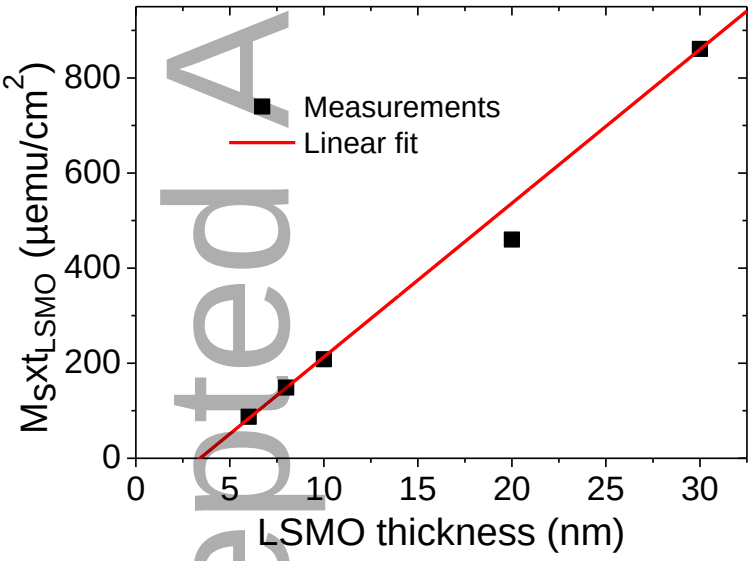

Fig. 3 : Belmeguenai et al.

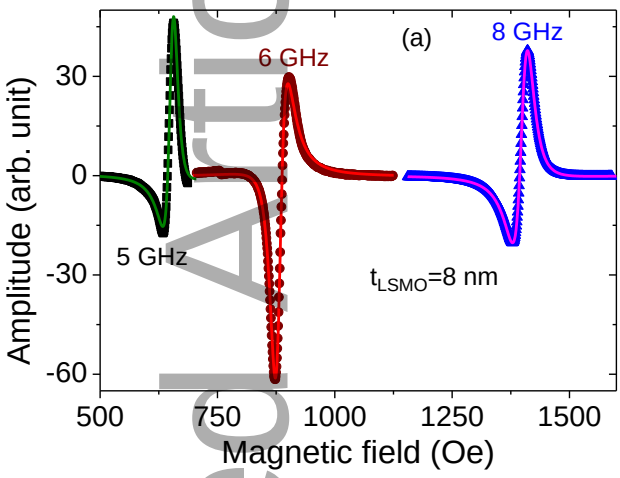

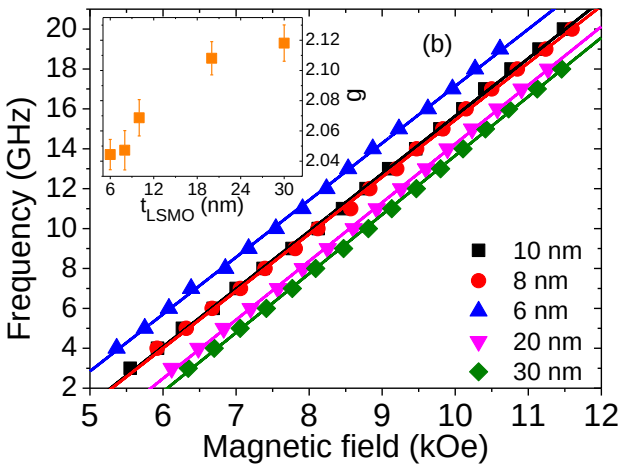

Fig. 4 : Belmeguenai et al.

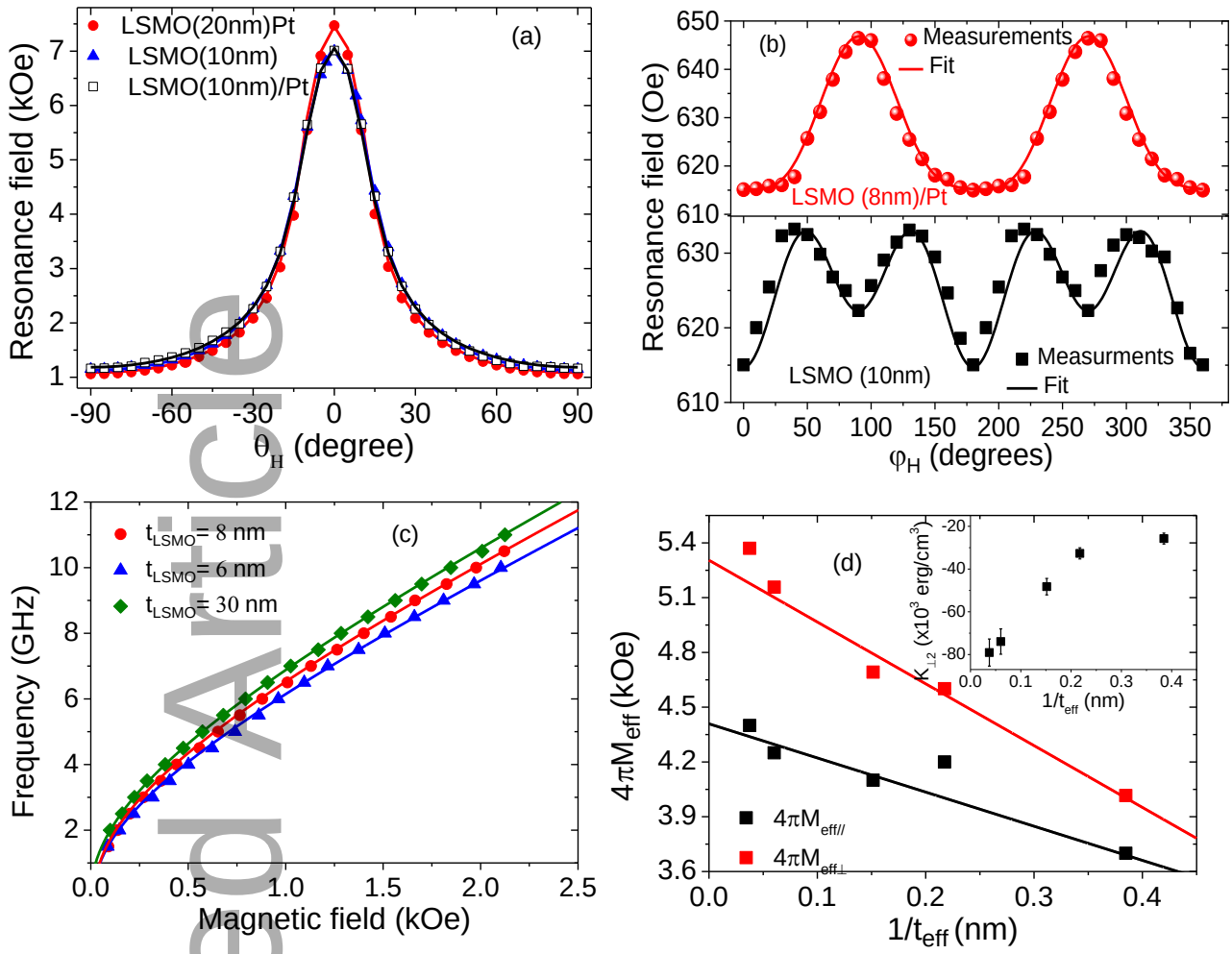

Fig. 5 : Belmeguenai et al.

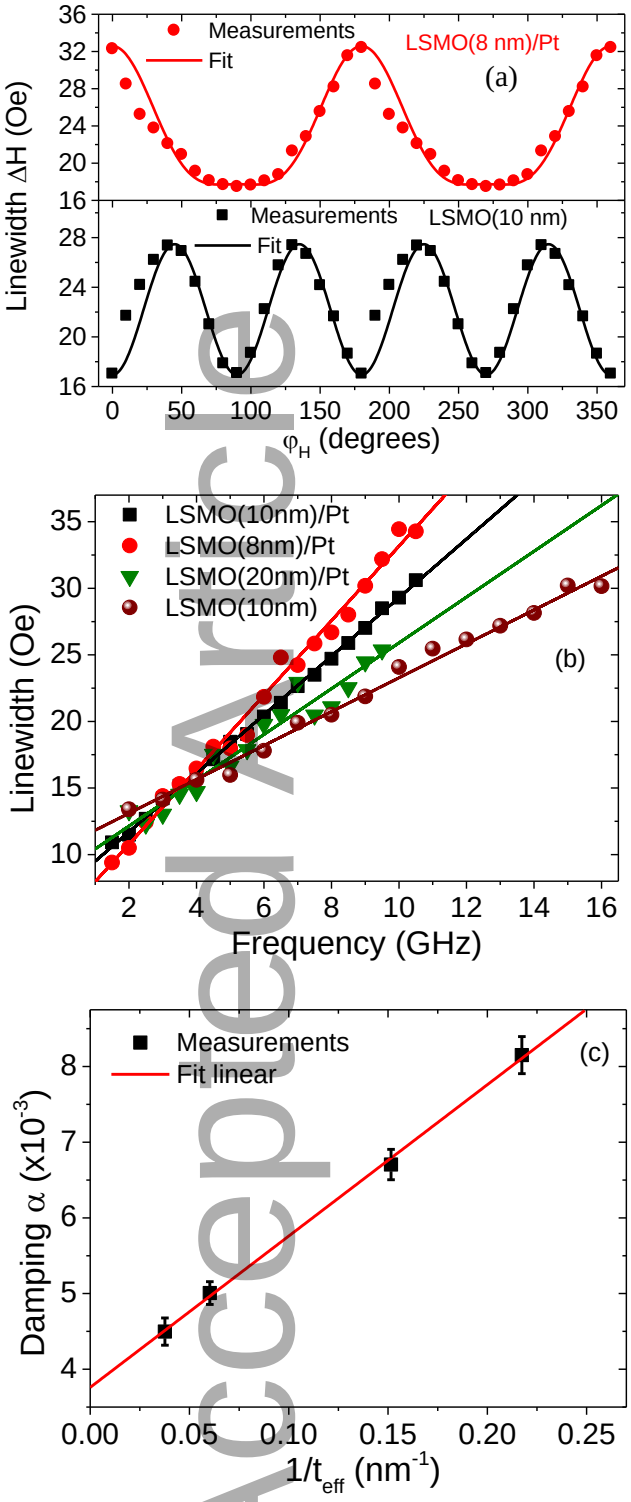

Figure captions

Figure 1: x-ray *2θ-ω* (out-of-plane) diffraction pattern using (Cu x-ray source) LSMO (30 nm)/Pt(7 nm) grown on STO (001) substrate.

Figure 2: Thickness dependence of the saturation magnetic moment per unit area for the LSMO/Pt systems of various thicknesses LSMO (t_{LSMO}) capped by the 7 nm thick Pt layer. Symbols refer to experimental data and solid lines are linear fits.

Figure 3: (a) Ferromagnetic resonance spectra (measured at different driven frequencies) representing the amplitude of the field derivative of the absorbed power as a function of the in plane applied magnetic field for the 8 nm thick LSMO film capped by a 7 nm thick Pt layer. Symbols refer to experimental data and solid lines are linear fits using equation (1) (b) Variation of the uniform precession mode frequency as a function of the perpendicularly applied magnetic field for LSMO/Pt(7 nm) for various thicknesses of LSMO. Symbols refer to experimental data and solid lines are linear fits using equation (2) with θ_M=θ_H=0°. The inset shows the g-factor as a function of the LSMO nominal thicknesses for LSMO/Pt films.

Figure 4: (a) Variations of the resonance field versus the out-of-plane angle (θ_H), measured at 7 GHz driven frequency, for LSMO (20 and 10 nm)/Pt systems and the reference 10 nm thick LSMO without Pt capping layer. θ_H refers to the out-of-plane angle defining the direction of the applied magnetic field and the normal to the film plane. Symbols refer to experimental data and solid lines are fits using equation (2). (b) FMR resonance field versus the direction of the in-plane applied magnetic field with respect to the substrate edge (φ_H) measured at 5 GHz driving frequency for LSMO(8 nm)/Pt system and the reference 10 nm thick LSMO without Pt capping layer. Symbols refer to experimental data and solid lines are fits using equation (3). (c) Variation of the uniform precession mode frequency as a function of the in-plane applied magnetic field for LSMO/Pt (7nm) with various LSMO thicknesses (t_{LSMO}). The magnetic applied field directions are $\varphi_H = 40°$, 90° and 50°, respectively for t_{LSMO}=6, 8 and 30 nm. Symbols refer to experimental data and solid lines are fits using equation (3). (d) Reciprocal LSMO effective thickness dependence of effective magnetizations $M_{eff//}$ and $M_{eff\perp}$ extracted from the fit of FMR measurements under in-plane and perpendicular applied magnetic fields, respectively for LSMO/Pt thin films, with in-plane and

perpendicularly applied magnetic field. Symbols refer to experimental data and solid lines are linear fits. The inset shows the dependence of the second order perpendicular anisotropy constant ($K_{\perp 2}$) as a function of the reciprocal LSMO effective thickness for LSMO/Pt systems.

Figure 5: (a) Dependence of the FMR half width at half maximum linewidth (ΔH) versus the direction of the in-plane applied magnetic field with respect to the sample edge (φ_H) measured at 5 GHz driving frequency for LSMO(8 nm)/Pt system and the reference 10 nm thick LSMO without Pt capping layer. Symbols refer to the experimental data and solid lines are linear fits using equation (4) and parameters of Table I. (b) Frequency dependence of the FMR linewidth (ΔH) for the LSOM/Pt system with various LSMO thicknesses and for the reference 10 nm thick LSMO without Pt capping layer. The magnetic applied field directions are φ_H= 90°, 40 and 60°, respectively for t_{LSMO}=8, 10 and 20 nm. For the reference sample, the measurements were acquired for φ_H =0°. Symbols refer to experimental data and solid lines are linear fits using equation (4). The applied magnetic field was applied in the direction where ΔH is minimal. (c) Gilbert damping constant as a function of the reciprocal LSMO effective thickness for LSMO/Pt films. Symbols refer to the experimental data and solid line is linear fit.

This work deals with the investigation of perpendicular magnetic anisotropy and spin pumping induced damping in $La_{2/3}Sr_{1/3}MnO_3$ (LSMO)/Pt systems. The magnetic damping coefficient varies linearly with the reciprocal LSMO effective thickness leading to relatively low spin mixing conductance of LSMO/Pt interface. Therefore, the low magnetization at saturation combined with the low Gilbert damping make LSMO/Pt good candidate for spintronic devices.